Astronomy & Astrophysics manuscript no. gulisano12˙ULYSSES˙expansion
April 8, 2012

Expansion of magnetic clouds in the outer heliosphere

A.M. Gulisano[1,2,3], P. Démoulin[4], S. Dasso[2,1], L. Rodriguez[5]

[1] Instituto de Astronomía y Física del Espacio, CONICET-UBA, CC. 67, Suc. 28, 1428 Buenos Aires, Argentina e-mail: agulisano@iafe.uba.ar, sdasso@iafe.uba.ar
[2] Departamento de Física, Facultad de Ciencias Exactas y Naturales, Universidad de Buenos Aires, 1428 Buenos Aires, Argentina e-mail: dasso@df.uba.ar
[3] Instituto Antártico Argentino (DNA), Cerrito 1248,CABA, Argentina
[4] Observatoire de Paris, LESIA, UMR 8109 (CNRS), F-92195 Meudon Principal Cedex, France e-mail: Pascal.Demoulin@obspm.fr
[4] Solar-Terrestrial Center of Excellence - SIDC, Royal Observatory of Belgium, Brussels, Belgium e-mail: rodriguez@oma.be

Received 2 january 2012; accepted 7 april 2012

ABSTRACT

Context. A large amount of magnetized plasma are frequently ejected from the Sun as Coronal Mass Ejections (CMEs). A part of these ejections are detected in the solar wind as magnetic clouds (MCs) which have flux rope signatures.
Aims. MCs are typically expanding structures in the inner heliosphere. The aim of this work is to derive the expansion properties of MCs in the outer heliosphere from 1 to 5 AU and to compare them to the ones in the inner heliosphere.
Methods. We analyze MCs observed by the Ulysses spacecraft using *in situ* magnetic field and plasma measurements. The MC boundaries are defined in the MC frame after defining the MC axis with a minimum variance method applied only to the flux rope structure. As in the inner heliosphere, a large fraction of the velocity profile within MCs is close to a linear function of time. This implies a self-similar expansion and a MC size that locally follows a power-law of the solar distance with an exponent called ζ. We derive the value of ζ from the *in situ* velocity data.
Results. We analyze separately the non-perturbed MCs (cases presenting a linear velocity profile almost for the full event), and perturbed MCs (cases presenting a strongly distorted velocity profile). We find that non-perturbed MCs expand with a similar non-dimensional expansion rate ($\zeta = 1.05 \pm 0.34$), i.e. slightly faster than the solar distance and than in the inner heliosphere ($\zeta = 0.91 \pm 0.23$). The subset of perturbed MCs expands, as in the inner heliosphere, with a significant lower rate and with a larger dispersion ($\zeta = 0.28 \pm 0.52$) as expected from the temporal evolution found in numerical simulations. This local measure of the expansion is also in agreement with the distribution with distance of MC size, mean magnetic field and plasma parameters. The MCs in interaction with a strong field region, e.g. another MC, have the most variable expansion rate (ranging from compression to over-expansion).

Key words. Sun: magnetic fields, Magnetohydrodynamics (MHD), Sun: coronal mass ejections (CMEs), Sun: solar wind, Interplanetary medium

1. Introduction

Magnetic clouds (MCs) are a subset of interplanetary coronal mass ejections, showing to an observer at rest in the heliosphere: a large and coherent rotation of the magnetic field vector, a magnetic field intensity larger than in their surroundings, and a low proton temperature (e.g., Klein & Burlaga 1982; Burlaga 1995). They transport huge helical magnetic structures in the heliosphere, and they are believed to be the most efficient mechanism to release magnetic helicity from the Sun (Rust 1994; Low 1997). They are also the most geoeffective events erupted from the Sun, and finally they are associated with observations of strong flux decrease of galactic cosmic rays (Tsurutani et al. 1988; Gosling et al. 1991; Webb et al. 2000; Cane et al. 2000; St. Cyr et al. 2000; Cane & Richardson 2003).

Despite the increasing interest to improve the knowledge of MCs from the last decades, there are still a lot of properties to unveil, as for instance their dynamical evolution while they travel in the solar wind (SW). In particular, during their evolution, MCs are in a significant expansion (e.g., Klein & Burlaga 1982; Farrugia et al. 1993). Observations of MCs at different heliodistances show that their radial size is increasing with the distance to the Sun (e.g., Kumar & Rust 1996; Bothmer & Schwenn 1998; Leitner et al. 2007). More generally, ICMEs are also known to have a global expansion in radial direction with heliodistance (e.g., Wang et al. 2005b; Liu et al. 2005). Then, the expansion properties of MCs and ICMEs differ significantly from the stationary Parker's solar wind.

From in situ observations of MCs, the plasma velocity profile is typically decreasing while the MC passes through the spacecraft, showing a faster speed at the beginning (when the spacecraft is going into the cloud, $V_{R,\mathrm{in}}$) and a slower speed at the end (when the spacecraft is going out the cloud, $V_{R,\mathrm{out}}$, e.g., Lepping et al. 2003; Gulisano et al. 2010). Moreover, the velocity profile inside MCs typically shows a linear profile, which is expected for a self similar expansion (Farrugia et al. 1993; Shimazu & Vandas 2002; Démoulin et al. 2008; Démoulin & Dasso 2009a). The time variation of the size of the full MC can be approximated with $\Delta V_{MC} = V_{R,\mathrm{out}} - V_{R,\mathrm{in}}$. However, a parcel of fluid a factor f times smaller than the MC would have typically a difference of velocity $\Delta V = f\ \Delta V_{MC}$ (because of the linear profile).

Send offprint requests to: A.M. Gulisano

Then, as ΔV is size dependent, it is not an intrinsic expansion rate of the parcels of fluid. Moreover, the regions near the MC boundaries are typically showing the strongest perturbations, so that ΔV is not a reliable measurement of the flux rope expansion rate.

In order to better measure the expansion of plasma in MCs, Démoulin et al. (2008) introduced a non-dimensional expansion rate (called ζ, see Sect. 4.1) which is computed from the local insitu measurements. It was shown that, if ζ is constant in time, then ζ is also determining the exponent of the selfsimilar expansion, i.e. the size of a parcel of fluid as $r(D) \sim r_0 D^{\zeta}$, with D the distance to the Sun.

From the analysis of the non-dimensional expansion rate (ζ) for a large sample of MCs observed in the inner heliosphere by the spacecraft Helios 1 and 2, Gulisano et al. (2010) found that there are two populations of MCs, one presenting a linear profile of the plasma velocity in almost all the passage of the cloud through the spacecraft (the non-perturbed subset) and another population presenting a strongly distorted velocity profile (the perturbed subset). The presence of the second population was interpreted as a consequence of the interaction of a fraction of the MCs with solar wind fast streams.

In the present paper we present an extension of the work by Gulisano et al. (2010) to the outer heliosphere from 1 to 5 AU, analysing observations made by the Ulysses spacecraft. We first describe the data used, the method to define the boundaries and the axis direction of the flux ropes, then the main characteristics of the velocity profile (Sect. 2). Next, we study statistically the dependence of the main MC properties in function of the solar distance (Sect. 3). Then, we analyze the expansion properties of MCs separately for perturbed and non-perturbed cases (Sect. 4). The MCs in interaction with a strong external magnetic field (such as with another MC) are analyzed separately case by case in Sect. 5. Finally, we summarize our results and conclude (Sect. 6).

2. Data and Method

2.1. Selected MCs

The aim of this work is to derive the generic expansion properties of MCs in the outer heliosphere. Then, we do not select MCs for their physical properties (e.g. driving a front shock or not), but rather studied a set of MCs as complete as possible in a given period of time. We selected the MCs previously analyzed by Rodriguez et al. (2004) for their thermal and energetic properties. This list of 40 MCs covers the time interval from February 1992 to August 2002. During the analysis of Ulysses data we found 6 extra MCs during this time interval. They are included at the end of Table A.1.

Present study has a different scope from Rodriguez et al. (2004) as our main aim is to quantify the expansion properties of MCs. We use data from the Solar Wind Observations Over the Poles of the Sun (SWOOPS, Bame et al. 1992) for plasma observations with a temporal cadence of 4 minutes. The magnetic field data are from the Vector Helium Magnetometer (VHM, Balogh et al. 1992); these observations have a temporal cadence of 1 second.

2.2. The MC frame

The magnetic and velocity fields observations are in the Radial Tangential Normal (RTN) system of reference ($\hat{\mathbf{R}}$, $\hat{\mathbf{T}}$, $\hat{\mathbf{N}}$). $\hat{\mathbf{R}}$ points from the Sun to the spacecraft, $\hat{\mathbf{T}}$ is the cross product of the Sun's rotation vector with $\hat{\mathbf{R}}$, and $\hat{\mathbf{N}}$ completes the right-handed system (e.g., Fränz & Harper 2002).

Another very useful system of coordinates is one attached to the local direction of the flux rope. In this MC local frame, $\hat{\mathbf{Z}}_{\rm cloud}$ is along the cloud axis (with $B_{\rm z,cloud} > 0$ in the MC central part). $\hat{\mathbf{Z}}_{\rm cloud}$ is found using the minimum variance (MV) technique to the normalized time series of the observed magnetic field (e.g. Gulisano et al. 2007, and references therein). We define $\hat{\mathbf{Y}}_{\rm cloud}$ in the direction $\hat{\mathbf{R}} \times \hat{\mathbf{Z}}_{\rm cloud}$ and $\hat{\mathbf{X}}_{\rm cloud}$ completes the right-handed orthonormal base ($\hat{\mathbf{X}}_{\rm cloud}$, $\hat{\mathbf{Y}}_{\rm cloud}$, $\hat{\mathbf{Z}}_{\rm cloud}$).

In the MC frame, the magnetic field components have a typical behavior as follow. The axial field component, $B_{\rm z,cloud}$, is typically maximum in the central part of the MC, and it declines toward the borders to small, or even negative, values. The component $B_{y,\rm cloud}$ has typically a main change of sign in the MC central part. When large fluctuations are present in some MCs, then $B_{y,\rm cloud}$ has an odd number of reversal (e.g. Steed et al. 2011). Finally, the component $B_{x,\rm cloud}$ is the weakest one if the spacecraft cross the central part of the MC; its relative magnitude provides an indication of the impact parameter (Gulisano et al. 2007; Démoulin & Dasso 2009b).

Another interest of the MC frame is that it permits to relate the in- and out-bounds of the crossed flux rope with the conservation of the azimuthal flux (Dasso et al. 2006). Neglecting the evolution of the magnetic field during the spacecraft crossing period (since the elapse time is small compared to the transit time from the Sun, see Démoulin et al. 2008 for a justification), we define the accumulative flux per unit length L along the MC axial direction as (Dasso et al. 2007):

$$\frac{F_y(t)}{L} = \int_{t_{\rm in}}^{t} B_{y,cloud}(t')\, V_{x,cloud}(t')\, {\rm d}t' \,, \qquad (1)$$

where $t_{\rm in}$ is the time of the front boundary. This time has been selected as a reference since the front boundary is usually well defined, however any other reference time can be used without any effect on the following conclusions. Since $B_{y,cloud}$ has a main change of sign inside a MC, $F_y(t)$ has a main extremum. It defines the time, called $t_{\rm center}$, which is approximately the time of closest approach to the flux rope center. With the hypothesis of local symmetry of translation along the main axis, the flux surface passing at the position of the spacecraft at t_1 is wrapped around the flux rope axis, and is observed at time t_2 defined by

$$F_y(t_1) = F_y(t_2) \,, \qquad (2)$$

from the conservation of the azimuthal flux. Within the flux rope, this equation relates any in-bound time to its conjugate in the out-bound.

2.3. Definition of the MC boundaries

As a first approximation, we choose the MC boundaries from the magnetic field in the RTN coordinate system taking into account the magnetic field properties (see Section 1). We also use the measured proton temperature compared to the expected temperature in the SW with the same speed (Lopez & Freeman 1986) including a dependence with solar distance (Wang et al. 2005b). However, a lower temperature than expected is only used as a guide, since we found that the magnetic field has sharper changes than the temperature, and so the magnetic field defines more precisely the flux rope boundaries.

The front, or in-bound, boundary of a MC is typically the easiest to determine. It is the limit between the fluctuating magnetic field of the sheath and the smoother field variation within

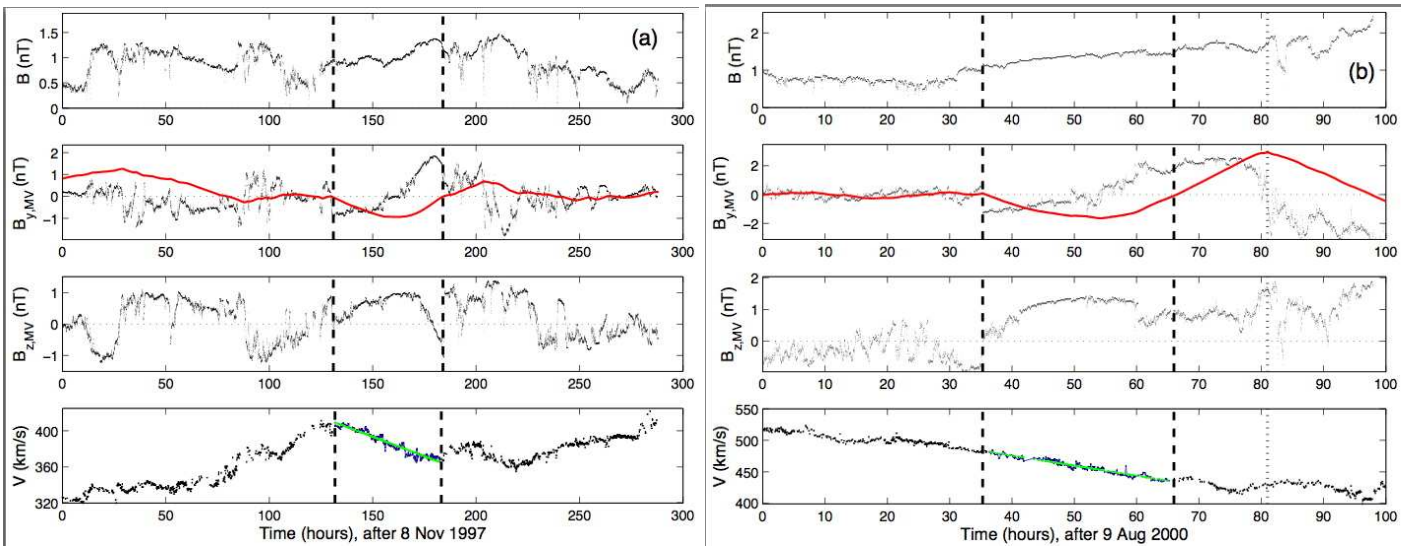

Fig. 1. Examples of two MCs with velocity profile not significantly perturbed (i.e. with an almost linear dependence with time). **(a)** MC 13 travels at low latitude (2°) at D = 5.3 AU in a slow SW and **(b)** MC 30 travels at high latitude (−66°) at D = 3 AU in a relatively slow SW for such high latitude. The vertical dashed lines define the MC (flux rope) boundaries, and the vertical dotted line defines the rear boundary of the MC back (Sect. 2.3, a back is only present on the right panels). The three top panels show the magnetic field norm and its two main components in the MC frame computed with the MV method (Sect. 2.2). $B_{z,MV}$ is the MC axial magnetic field component. $B_{y,MV}$ is the magnetic field component both orthogonal to the MC axis and to the radial direction from the Sun ($\hat{\mathbf{R}}$). The solid red line represents F_y, which is the accumulated flux of $B_{y,MV}$ [Eq. (1)]. The bottom panel shows the observed velocity component in the radial direction ($\hat{\mathbf{R}}$). A linear least square fit of the velocity (green line) is applied in the time interval where an almost linear trend is present within the MC.

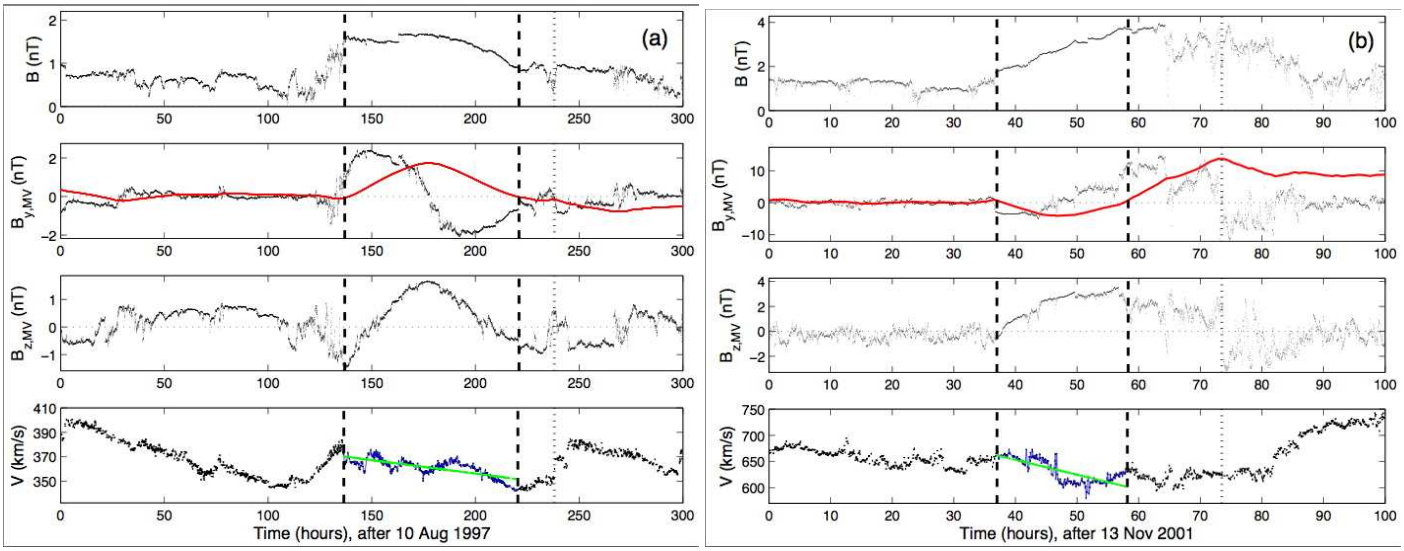

Fig. 2. Examples of two MCs with perturbed velocity (i.e. deviating from a linear function of time). **(a)** MC 11 travels at low latitude (6°) at D = 5.2 AU in a slow SW and **(b)** MC 36 travels at high latitude (75°) at D = 2.3 AU in a fast SW. The same quantities and drawing convention than in Fig. 1 are used.

the flux rope. A current sheet is typically present between these two regions, and the front boundary is set there, at a time noted t_{in}.

The rear, or out-bound, boundary is more difficult to define, in particular since many MCs have a back region which have physical properties intermediate between MC and SW properties, so that the transition between the flux rope and the perturbed SW is frequently not as sharp as at the in-bound boundary. Dasso et al. (2006, 2007) concluded that this back region is formed, during the transit from the Sun, by reconnection of the flux rope with the overtaken magnetic field. We use the conservation of the azimuthal flux between the in- and out-bound, Eq. (2), to define the out-bound boundary. When a back region is present, the time t_{out} of the out-bound boundary is defined as the first solution of $F_y(t_{out}) = F_y(t_{in}) = 0$. However, this condition depends on the determination of the MC frame so that an iterative procedure is needed, as follows.

We start with approximative MC boundaries defined in the RTN system, then we perform a MV analysis to find the local frame of the MC. Next, we analyze the magnetic field components in the local frame, and redefine the boundaries according to the azimuthal flux conservation expected in a flux rope [Eq. (2)]. In most cases the temporal variation of the magnetic components indicate that the rear boundary needs to be changed

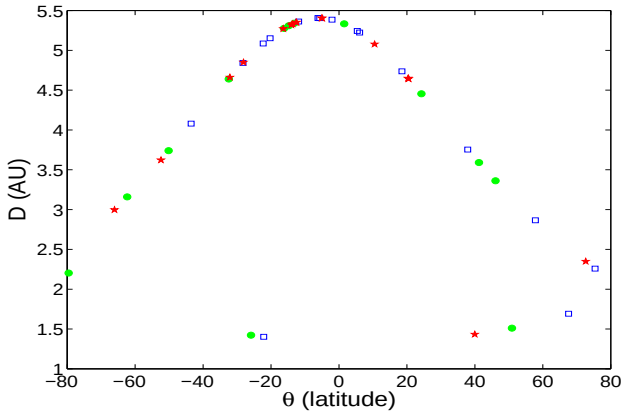

Fig. 3. Spatial localization of the MCs listed in Table A.1. The MCs are separated in three groups: non-perturbed (filled green circles), perturbed (empty blue squares), and in interaction (red stars).

of location. Then, the MV analysis is performed only on the flux rope interval. This is an important step since an excess of magnetic flux on one side of the flux rope is typically introducing a systematic bias in the MV directions. Finally, we perform the same procedure iteratively until convergence is achieved. This defines improved boundaries and orientation of the flux rope.

As at the front boundary, a current sheet is expected at the out-bound boundary (since it separates two regions with different origins and physical properties). Indeed, a current sheet is typically found in the vicinity of the time $t_{\rm out}$ in most MC analyzed. The bending of the flux rope axis is one plausible cause of the small difference in time between $t_{\rm out}$ and the closest current sheet.

In the out-bound branch of a few MCs, $B_{y,\rm cloud}$ has an important current sheet and later on fluctuate before $F_y(t)$ vanishes. This indicates a deficit of azimuthal flux in the out-bound branch compared to the in-bound one. In such case, $t_{\rm out}$ is defined by the observed time of the current sheet, and the flux rope extension is in the time interval $[t_{\rm in}, t_{\rm out}]$ where $t_{\rm in}$ is redefined by $F_y(t_{\rm in}) = F_y(t_{\rm out})$. The iterative procedure described above is then applied to improve $t_{\rm in}$ and the flux rope orientation.

2.4. MC groups

In the working line of Gulisano et al. (2010), we split the data set in three groups: non-perturbed MCs, perturbed MCs and MCs in interaction (noted interacting).

The interacting group contains the MCs which have a strong magnetic field nearby (e.g. another MC). From MHD simulations their physical properties are expected to be significantly different than non-interacting MCs (e.g., Xiong et al. 2007). Indeed, observations confirm that MCs in interaction could have different behavior than non-interacting MCs (e.g. Wang et al. 2005a; Dasso et al. 2009).

MCs in the non-perturbed and perturbed groups have a less disturbed surroundings than MCs of the interacting group. MCs in the non-perturbed group have an almost linear velocity profile in more than 75% of the flux rope, while in the perturbed MCs this condition is not satisfied. Two examples of each group are shown in Figs. 1,2, the label (number), the group, and the main properties of each MC are given in Table A.1.

Table 1. Exponents e in the fit with a power law D^e for S, $< B >$ and $< N_{\rm p} >$ (found with linear fit in log-log plots, Fig. 4).

range of D [a]	S [b]	$< B >$ [b]	$< N_{\rm p} >$ [b]	Ref.[c]
all MCs				
[1.4, 5.4]	0.49±0.26	−1.20±0.20	−1.70±0.34	1
non-perturbed and perturbed MCs				
[0.3, 1]	0.78±0.12	−1.85±0.07		2
[1.4, 5.4]	0.56±0.34	−1.18±0.27	−1.70±0.43	1
non-perturbed MCs				
[0.3, 1]	0.89±0.15	−1.85±0.11		2
[1.4, 5.4]	0.79±0.46	−1.39±0.92	−2.24±0.66	1
perturbed MCs				
[0.3, 1]	0.45±0.16	−1.89±0.10		2
[1.4, 5.4]	0.54±0.48	−1.14±0.26	−1.40±0.50	1
MCs				
[0.3, 1]			−2.40±0.30	3
[0.3, 1]	1.14±0.44	−1.64±0.40	−2.44±0.46	4
[0.3, 4.]	0.97±0.10	−1.80	−2.8	5
[0.3, 4.8]	0.78±0.10			3
[0.3, 5.4]	0.61±0.09	−1.30±0.09	−2.62±0.07	4
[1.4, 5.4]		−0.88±0.22		4
ICMEs				
[0.3, 5.4]	0.61	−1.52		6
[0.3, 5.4]	0.92±0.07	−1.40±0.08	−2.32±0.07	7

[a] The range of solar distances is in AU. In the middle part of the table, MCs are separated in non-perturbed and perturbed MCs.
[b] The exponents, e, are given for the size S in the $\hat{\mathbf{R}}$ direction, the mean magnetic field strength $< B >$, and the mean proton density $< N_{\rm p} >$. All quantities are computed within the flux rope boundaries.
[c] We compare our results with our previous results in the inner heliosphere and with other studies of MCs and ICMEs. The results are from: 1: present work, 2: Gulisano et al. (2010), 3: Bothmer & Schwenn (1998), 4: Leitner et al. (2007), 5: Kumar & Rust (1996), 6: Wang et al. (2005b), 7: Liu et al. (2005).

3. MC size and mean properties

The aim of this section is to analyze the size and mean properties, along the spacecraft trajectory, of MCs in function of the solar distance D. Because of the trajectory of Ulysses, a correlation between D and the absolute value of the latitude is present in the analyzed data (Fig. 3). However, we do not find significant differences in the following results when MCs are grouped by latitudes, so that this correlation between D and latitude does not affect our conclusions. All the studied properties are affected by the expansion achieved from the Sun to Ulysses. From models (see e.g., Chen 1996; Kumar & Rust 1996; Démoulin & Dasso 2009a), all properties are expected to have a power law dependence with D, then we perform a linear fit for each property plotted in log-log scale (Figs. 4,5), for the non-perturbed and perturbed groups. Since MCs in interaction are strongly case dependent, their properties are not compared (fitted) with global models here.

3.1. MC size

With the MC boundaries defined in Sect. 2.3, we compute the size S in the direction $\hat{\mathbf{R}}$ as the product of the duration of the MC and its velocity at closest approach to the center of the flux rope. Compared to most previous works, see Sect. 1, this defines typically a smaller size as the back region is not included.

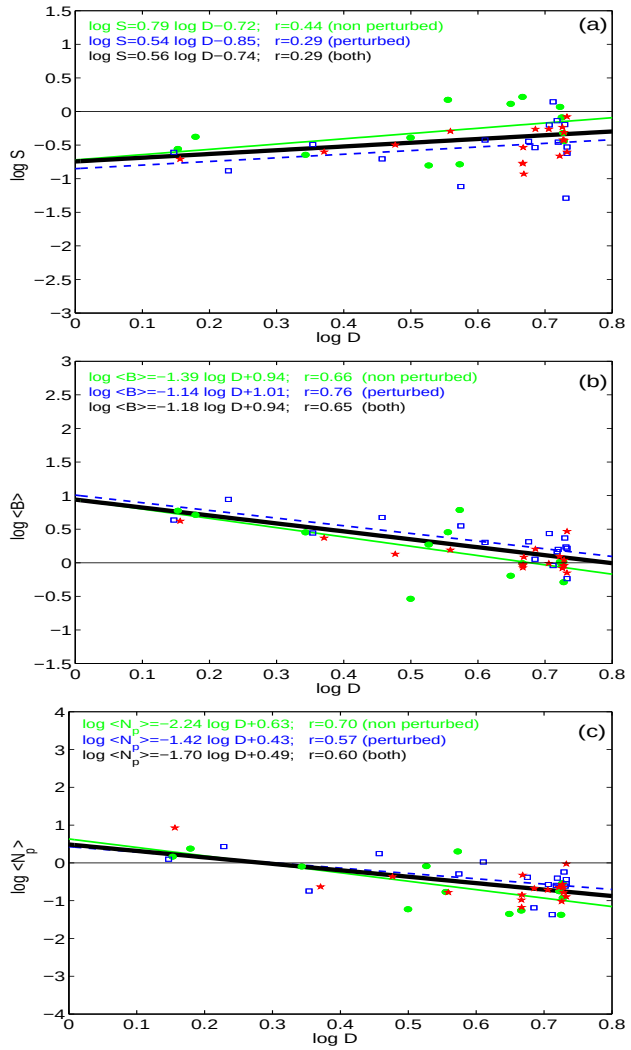

Fig. 4. Dependence with the solar distance, D in AU, of **(a)** the radial size in the $\hat{\mathbf{R}}$ direction (AU), **(b)** the mean magnetic field strength (nT), and **(c)** the mean proton density (cm^{-3}) with log-log plots. The MCs are separated in three groups: non-perturbed (filled green circles), perturbed (empty blue squares), and in interaction (red stars). The straight lines are the result of a least square fit for non-perturbed (thin continuous green line), perturbed (dashed blue line), and for non-perturbed and perturbed MCs (thick continuous black line). The fits and the absolute value of the correlation coefficients, r, are added at the top of each panel.

Since the majority of previous studies include all MCs independently of the groups we defined above, we first compare them to our results with all MCs included (Table 1). In the range [1.4,5.4] AU, we found an exponent lower (0.49 ± 0.26) than previous studies on MCs or ICMEs in the inner and outer heliosphere (lower part of Table 1). Taking into account only non-perturbed and perturbed MCs, the exponent is slightly higher (0.56 ± 0.34), but still below previous studies, including our previous result obtained with Helios data (0.78 ± 0.12).

Next, we analyze separately the non-perturbed and perturbed MCs. In the range [1.4,5.4] AU, we found comparable exponents to our previous results obtained with Helios data both for **non-perturbed** and perturbed MCs (Table 1). Perturbed MCs have a significantly lower size in average than non-perturbed MCs and this tendency is increasing with solar distance (Fig. 4a). We found that perturbed MCs have typically a smaller size S, by a factor ≈ 1.3, than non-perturbed MCs.

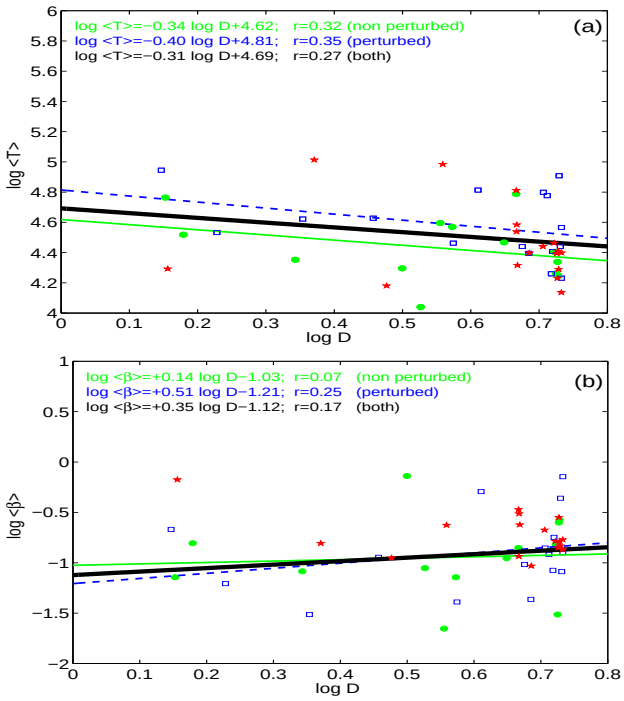

Fig. 5. Dependence with the solar distance, D in AU, of **(a)** the mean proton temperature $< T_p >$ (K) and **(b)** the mean proton β. The drawing convention is the same than in Fig. 4.

The MCs in interaction (interacting MCs) have typically a lower size S than the non-perturbed MCs (Fig. 4a). We interpret this result as a direct effect of the compression and/or reconnection with the interacting MC or strong magnetic field structure.

3.2. Magnetic field strength

We define the average field $< B >$ within the flux rope boundaries defined in Sect. 2.3 and proceed as above with S. $< B >$ is decreasing significantly slower with distance in the Ulysses range (-1.18 ± 0.27) than in the Helios range (-1.85 ± 0.07) for the non-perturbed and perturbed MCs (a similar result is obtained when also including the **interacting** MCs). Finally, combining our Helios and Ulysses results, we have an intermediate exponent (-1.5 ± 0.1). This last result is closer to the results of Wang et al. (2005b) and Liu et al. (2005) obtained from a larger set of ICMEs in the same range of distance (bottom of Table 1).

The non-perturbed MCs have a slightly steeper decrease of magnetic field strength with distance than the perturbed MCs (Fig. 4b). This result is coherent with the conservation of magnetic flux combined with a slightly larger increase of size with distance of the non-perturbed MCs compared to the perturbed ones. We also found that the perturbed MCs have typically a stronger magnetic field, by a factor between ≈ 1.4 and 1.7, than non-perturbed MCs (Fig. 4b), a result coherent with a smaller expansion rate for perturbed MCs (see Sect. 3.1 and 4.3).

The effect of the interaction on $< B >$ is weaker than for the size S. There is only a weak tendency for interacting MCs to have stronger $< B >$ than non-perturbed MCs (Fig. 4b).

3.3. Proton density

We define the average proton density $< N_p >$ as above for the magnetic field strength, i.e. within the flux rope boundaries. For the non-perturbed and perturbed MCs, the density decreases sig-

Table 2. Average and dispersion of the main parameters of MCs from from present study and Du et al. (2010).

Group [a]	V_c [b] km/s	$S_{1\,AU}$ [c] AU	$< B >_{1\,AU}$ [c] nT	$< N_p >_{1\,AU}$ [c] cm^{-3}	$< \beta_p >$	γ [d] $^\circ$	ζ [e]
all MCs	470±110	0.16±0.12	12±7	9±8	0.19±0.17	68±17	0.77±0.75
non-perturbed and perturbed	480±120	0.18±0.14	14±8	9±8	0.18±0.19	68±20	0.63±0.59
non-perturbed	480±130	0.24±0.16	11±9	7±10	0.17±0.18	63±24	1.05±0.34
perturbed	480±110	0.13±0.09	16±6	11±7	0.19±0.20	72±15	0.28±0.52
interacting	470±130	0.12±0.05	10±6	9±9	0.22±0.14	66±13	1.00±0.93
MC[f]	500±100	0.26±0.19	11±6				0.59±0.51
non-MC ICME[f]	480± 90	0.22±0.21	5±4				0.68±0.48

[a] The MCs are separated in three groups: non-perturbed, perturbed, and in interaction (interacting).
[b] V_c is the velocity at the closest distance from the MC center.
[c] The size and the mean field are normalized to 1 AU according to Eq. (8) and the proton density with $< N_p >_{1\,AU} = < N_p > D^{2.2}$ where D is the solar distance in AU.
[d] γ is the angle between the MC axis and the radial direction ($\hat{\mathbf{R}}$).
[e] ζ is the nondimensional expansion rate [Eq. (5)].
[f] Computed from the results of Du et al. (2010).

nificantly less rapidly with distance (exponent $= -1.70 \pm 0.43$) than in previous studies (exponents in the range $[-2.8, -2.3]$) both for the inner heliosphere and the combination of inner and outer heliosphere. However, we are not aware of results for the outer heliosphere alone (apart Fig. 10 of Leitner et al. 2007, but no fit is provided).

Nevertheless, for the non-perturbed MCs the density decreases with D with a power-law closer to previous studies. In contrast, for perturbed MCs the density decreases much slower with distance. This is qualitatively in agreement with a lower expansion of S and a lower decrease of $< B >$ with D, while the difference between non-perturbed and perturbed MCs is more important for the average proton density. Even if there is a qualitative agreement, the systematic lower decrease of $< N_p >$ with D than in previous studies could be related to an important variability of N_p in MCs (e.g. at 1 AU see Lepping et al. 2003) so that $< N_p >$ is case dependent and could be biased with our relatively low number of MCs. When the same MC is observed at two distances, this bias is removed. For MC 15 we obtained a larger slope of 2.9 by using the mean observed density at ACE and Ulysses (Nakwacki et al. 2011).

The effect of the interaction on $< N_p >$ is weak, comparable to the effect on $< B >$. There is only a weak tendency for interacting MCs to have stronger $< N_p >$ than non-perturbed MCs (Fig. 4c). While there is too few interacting MCs at low D to give a strong conclusion, the tendency of a global decrease of $< N_p >$ with D is dominant over the effect (typically compression) of an interaction with another MC or a strong B region.

3.4. Proton temperature

The average proton temperature is only weakly decreasing with distance (Fig. 5a). The non-perturbed and perturbed MCs have a dependence close to $D^{-0.34}$ and $D^{-0.40}$, respectively. This contrasts with the decrease found in the SW, typically around $D^{-0.7}$ (Gazis et al. 2006; Richardson & Cane 1995). Moreover, the MCs in interaction are not significantly hotter than non-perturbed and perturbed MCs (apart two hot interacting MCs, Fig. 5a).

The result above also differs with the decrease of temperature as $\approx D^{-1.6}$ found by Leitner et al. (2007) for MCs observed in the range $[0.3, 5.4]$ AU. However, our results are coherent with Leitner et al. (2007) since their Fig. 11 shows no decrease of proton temperature with distance for MCs observed Ulysses. We conclude, in agreement with previous results, that the proton temperature of MCs in the outer heliosphere is decreasing with D much slower than in the inner heliosphere and than in the SW.

Moreover, MCs have a larger volume expansion than the SW, the main difference being that MCs expand significantly in the radial direction (Table 1 and Fig. 6 below) in contrast with the SW which has no mean radial expansion. Considering an adiabatic expansion implies that MCs should become even cooler than the SW with distance. The opposite is in fact observed, which implies a much larger heating input in the MCs than in the SW. A significant part of this heating could come from a turbulent cascade to small scales. Because $\beta_p << 1$ in MCs (see next subsection), the dissipation of a small fraction of the magnetic energy provides a large increase of the plasma temperature, while the same amount of magnetic energy in the SW provides only a small increase of the plasma temperature ($\beta_p \approx 1$).

3.5. Proton plasma β

The proton plasma β, noted β_p, is defined as the ratio of the proton thermal pressure to the magnetic pressure. Thus, if the decay of the proton density, proton temperature, and magnetic field intensity, are real power laws (respectively, $N_p \propto D^{-n_n}$, $T_p \propto D^{-n_T}$, and $B \propto D^{-n_B}$), the decay of β_p, will be $\beta_p \propto D^{-n_n - n_T + 2n_B}$, which in our Ulysses study corresponds to an expected increasing function with the heliodistance, such as $\beta_{p,exp} \propto D^{-1.7-0.31+2*1.18} \sim D^{+0.35}$ for the combined sample of **non-perturbed** and perturbed MCs (Figs. 4b,c, 5a). Another estimation can be realized by supposing an isotropic expansion of MCs with distances increasing as D^m. Using the conservation of mass and of magnetic flux (i.e., in an ideal regime), we theoretically expect an evolution such that $\beta_p \propto D^{-3m-n_T+4m}$, which is $\beta_p \propto D^{+0.25}$ for non-perturbed and perturbed MCs and $\beta_p \propto D^{+0.45}$ for non-perturbed MCs, then comparable to the previous estimation.

We computed the mean value of β_p inside each studied cloud. $< \beta_p >$ is lower than unity for all MCs in our sample, and it has a tendency to slightly increase with solar distance for non-perturbed **and** perturbed MCs. We find that $\beta_p \propto D^{0.35}$ for the combined groups of MCs (Fig. 5b), so a very similar dependance than found above assuming exact power laws.

Leitner et al. (2007) found a slight decrease, $\approx D^{-0.4}$, for MCs in the range $[0.3, 5.4]$ AU. Still, this global tendency is not

present for MCs observed with Ulysses as their Fig. 12 shows a tendency of increasing β_p with D. Then, we conclude that β_p has a different dependence with D in the inner and outer heliosphere.

Next, we analyze separately the dependence of β_p with D for each MC group. β_p is almost independent of D for the **non-perturbed** MCs, and the above growing tendency with distance is mainly due to the perturbed MCs. The MCs in interaction have typically a larger β_p at all D (Fig. 5b).

4. Expansion rate of MCs

MCs have typically a velocity profile close to a linear function of time with a larger velocity in the front than at the rear. So MCs are expanding magnetic structures as they move away from the Sun. In this section we characterize their expansion rate.

4.1. Non-dimensional expansion rate

The measured temporal profile $V_R(t)$ of each MC is fitted using a least square fit with a linear function of time,

$$V_{R,\mathrm{fit}}(t) = V_{\mathrm{o,fit}} + (\mathrm{d}V_R/\mathrm{d}t)_{\mathrm{fit}}\, t\,, \tag{3}$$

where $(\mathrm{d}V_R/\mathrm{d}t)_{\mathrm{fit}}$ is the fitted slope. We always keep the fitting range inside the flux rope, and restricts it to the most linear part of the observed profile. The observed linear profile of V_R indicates that different parts of the flux rope expands at about the same rate in the direction $\hat{\mathbf{R}}$.

The linear fit is used to define the velocities $V_{R,\mathrm{fit}}(t_{in})$ and $V_{R,\mathrm{fit}}(t_{out})$ at the flux rope boundaries (Sect. 2.3). Then, we define the full expansion velocity of a flux rope as:

$$\Delta V_R = V_{R,\mathrm{fit}}(t_{in}) - V_{R,\mathrm{fit}}(t_{out})\,. \tag{4}$$

For not perturbed MCs, ΔV_R, is very close to the observed velocity difference $V_R(t_{in}) - V_R(t_{out})$, see e.g. the lower panels of Fig. 1. For perturbed MCs, this procedure minimizes the effects of the perturbations present inside the flux rope and especially close to the MC boundaries.

Following the works of Démoulin & Dasso (2009a) and Gulisano et al. (2010), we define the non-dimensional expansion rate as:

$$\zeta = \frac{\Delta V_R}{\Delta t}\frac{D}{V_c^2}\,. \tag{5}$$

ζ defines a scaling law for the size S of the flux rope (along $\hat{\mathbf{R}}$) with the distance (D) from the Sun as $S \propto D^{\zeta}$. This simple interpretation of ζ is obtained with the following two simplifications (justified in Démoulin & Dasso 2009a). Firstly, we neglect the aging effect (the front is observed at an earlier time than the rear, so when observed at the front the flux rope is smaller than when it is observed at the rear), and secondly, ζ is approximately constant during the time interval of the observed flux rope.

Then, while ζ is a local measurement inside the flux rope, it provides a measure of the exponent m of the flux rope size if it follows a power law:

$$S = S_0\left(\frac{D}{D_0}\right)^m\,. \tag{6}$$

Indeed, taking the temporal derivative of S:

$$\frac{\mathrm{d}S}{\mathrm{d}t} = \Delta V_R = \frac{\mathrm{d}S}{\mathrm{d}D}\frac{\mathrm{d}D}{\mathrm{d}t} \approx m\frac{S}{D}V_c \approx m\frac{\Delta t V_c^2}{D}\,. \tag{7}$$

Then, we found a relation equivalent to Eq. (5), so for self-similarly expanding MCs we have $m \approx \zeta$.

4.2. Expansion of non-perturbed MCs

The main driver of MCs expansion was identified as the rapid decrease of the total SW pressure with solar distance by Démoulin & Dasso (2009a). They have followed the force-free evolution away from the Sun of flux ropes with a variety of magnetic field profiles and with ideal MHD or with full resistive relaxation under the preservation of magnetic helicity. Within this theoretical framework, they have shown that a force-free flux rope has an almost self similar expansion, so a velocity profile almost linear with time as observed by a spacecraft crossing a MC (e.g. Figs. 1,2). With a total SW pressure behaving as D^{-n_P}, they also found that the normalized expansion rate is $\zeta \approx n_P/4$. These results apply to a progressive evolution of a flux rope in a quiet SW, so the non-perturbed MCs are expected to have properties the closest to these theoretical results.

The mean value of ζ for non-perturbed MCs, observed in the range [1.4, 5.4] AU, is $<\zeta> \approx 1.05 \pm 0.34$. This is slightly above the mean values, $\approx 0.80 \pm 0.18$ and $\approx 0.91 \pm 0.23$, found at 1 AU and in the range [0.3, 1.] AU, respectively (Démoulin et al. 2008; Gulisano et al. 2010). This is a small increase in comparison to the change of D, which is a factor in the definition of ζ [Eq. (5)]. Since V_c has no significant dependence with D (Wang et al. 2005b), the increase of D is compensated mainly by the decrease of $\Delta V_R/\Delta t$.

The slightly larger mean $<\zeta>$ in the range [1.4, 5.4] AU is mostly due to larger ζ values found at lower D values (Fig. 6a), so in the region the closest to both previous studies. In fact, due to the characteristics of Ulysses orbit, there are only a few observed MCs for $D < 3$ AU (Fig. 3) so that the decrease with D of the linear fit of ζ could be due to the specific properties of the few detected MCs at these lower distances. We also recall that D is strongly correlated to the heliolatitude $|\theta|$, Fig. 3, so that the dependence $\zeta(D)$ shown in Fig. 6a could be also an effect of latitude. Still, we emphasize that the $<\zeta>$ found here with Ulysses is only slightly larger than the values found previously at lower helio-distances. These differences are small compared to the significantly different SW properties of the slow and fast SW dominantly present at low and high latitude, respectively.

As in the previous study, we test the possible dependence of ζ on the MC properties. Both the MC size and field strength strongly change with D (Fig. 4a,b). We use the fits found for the non-perturbed MCs to remove, in average, the evolution with D. So we define values at a giving solar distance, here taken at 1 AU, with the relations:

$$\begin{aligned} S_{1\,\mathrm{AU}} &= S\, D^{-0.79} \\ <B>_{1\,\mathrm{AU}} &= <B>\, D^{+1.39}\,. \end{aligned} \tag{8}$$

The mean MC speed is only weakly evolving with D in the outer heliosphere (see e.g. Wang et al. 2005b, for a large set of ICMEs, including MCs), so we use below the measured velocity of the center V_c.

We find that for non-perturbed MCs ζ is almost independent of $<B>_{1\,\mathrm{AU}}$ (Fig. 6d) as it was found in the range [0.3, 1.] AU (compared to Fig. 4d of Gulisano et al. 2010). A small difference is that ζ decreases slightly with V_c and $S_{1\,\mathrm{AU}}$ (Fig. 6b,c) while a nearly constant value was found in the range [0.3, 1.] AU (compared to Fig. 4b,c of Gulisano et al. 2010). This difference is probably not due to a latitude dependence since the MCs observed at $|\theta| < 25°$ or $> 25°$ are evenly distributed in the three plots when we analyzed the two groups independently [not shown], so similar results are obtained. Finally, using other exponents in Eq. (8), in the range given in Table 1, induces only

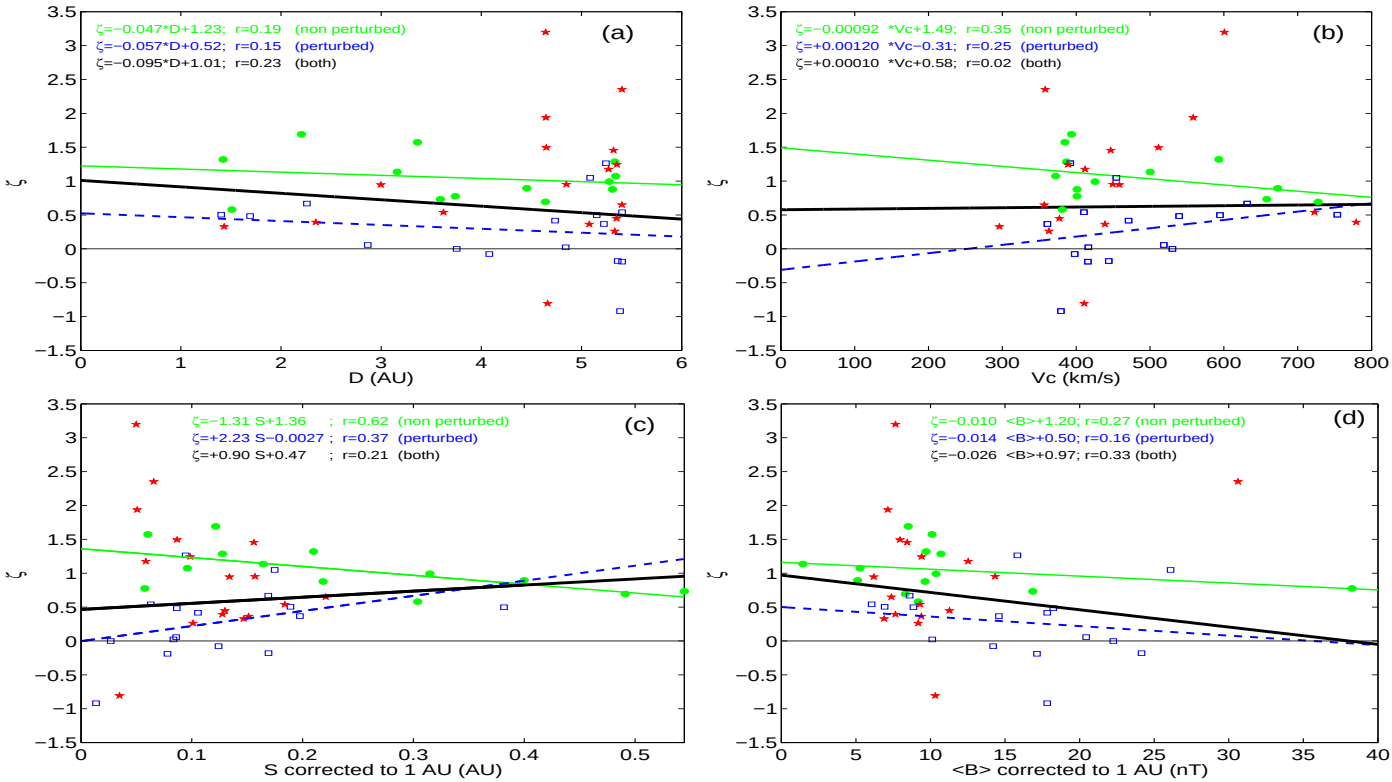

Fig. 6. The panels **(a-d)** show the correlation analysis that tests for the dependence of the non-dimensional expansion factor ζ [Eq. (5)] as a function of other MC parameters. The drawing convention is the same than in Fig. 4. $S_{1\,\mathrm{AU}}$ and $< B >_{1\,\mathrm{AU}}$ are normalized to 1 AU using the size and field strength dependence on the distance, according to the relationship given in Figure 4 for non-perturbed MCs, see Eq. (8).

slight changes in the linear fits shown in Fig. 6, in particular in the magnitude of the slope.

4.3. Expansion of perturbed MCs

A main difference of perturbed MCs, compared to the non-perturbed ones, is their lower expansion rate and a larger dispersion, $< \zeta >= 0.28 \pm 0.52$, compared to $< \zeta >= 1.05 \pm 0.34$ for non-perturbed MCs (see also Fig. 7c,d). These results are comparable to the results found in the distance range [0.3, 1] AU by Gulisano et al. (2010) since they found $< \zeta >= 0.48 \pm 0.79$ and $< \zeta >= 0.91 \pm 0.23$ for perturbed and non-perturbed MCs, respectively (Fig. 7a,b). This lower expansion rate for perturbed MCs is indeed expected from MHD simulations if the origin of the perturbation is an overtaking magnetized plasma since it is compressing the MC, so decreasing its expansion rate (Xiong et al. 2006a,b).

A significant overtaking flow, with a velocity larger than at the front of the MC, is found in 12 over 20 perturbed MCs. These strong flows are located behind the observed MC, and typically a shock, or at least a rapid variation of V, is present at the rear boundary of the back region, as illustrated by MC 11 in Fig. 2a. This is a main difference with MCs observed in the range [0.3, 1] AU, as the overtaking flow was typically entering deeply in the perturbed MCs, and moreover, a strong shock was typically present inside the perturbed MC (compare Fig. 2a with Fig. 2 Gulisano et al. 2010). This difference can be interpreted with the MHD simulations of Xiong et al. (2006a,b), as follows. The observations at Helios distances correspond to the interacting stage when the overtaking shock is traveling inside the MC (e.g. see Fig. 5 of Xiong et al. 2006a). At larger solar distances, the overtaking shock has exit from the front of the MC, so it is not observed inside the MC with Ulysses data. Still, a part of the overtaking flow is present behind the MC. Then, the compression of the overtaking flow is still present, and most perturbed MCs are under-expanding.

Another evidence of a different evolution stage at Ulysses compared with Helios is that ζ shows no significant dependence on D (Fig. 6a), while the mean tendency of ζ was to increase with D and to reach the $< \zeta >$ at 1 AU of unperturbed MCs for Helios MCs (Fig. 4a Gulisano et al. 2010).

Only one perturbed MC is expanding slightly faster than the mean expansion rate of unperturbed MCs (Fig. 6), while a stronger over expansion is present in some MCs in interaction. Indeed, such over expanding flux ropes are found in the above MHD simulations in the late stage of evolution, as follows. The overtaking magnetized plasma progressively flows on the MC sides and overtakes the MC. When only a weak overtaking flow remains at the MC rear, the expansion rate could increase. Indeed, the MC internal magnetic pressure is larger (due to the previous compression) than the pressure value for another MC at the same position and with no overtaking flow before. This over pressure drives a faster MC expansion (e.g. see the summary of two simulations in Fig. 7 of Xiong et al. 2006a). So the expansion rate of perturbed MCs depend on the interaction stage they are observed, see the cartoon in Figure 6 of Gulisano et al. (2010).

Some properties of ζ for perturbed MCs are still similar in the inner and outer heliosphere. ζ shows an increase with both V_c and $S_{1\,\mathrm{AU}}$ (Fig. 6b,c), and a decrease with $< B >_{1\,\mathrm{AU}}$ (Fig. 6d) as found with Helios data (Fig. 4b,c,d Gulisano et al. 2010). However, the slopes are smaller by a factor $\approx 2, 2$, and 6 respectively. Finally, it is worth noting that the above differences are not due to a difference in the range of parameters since V_c,

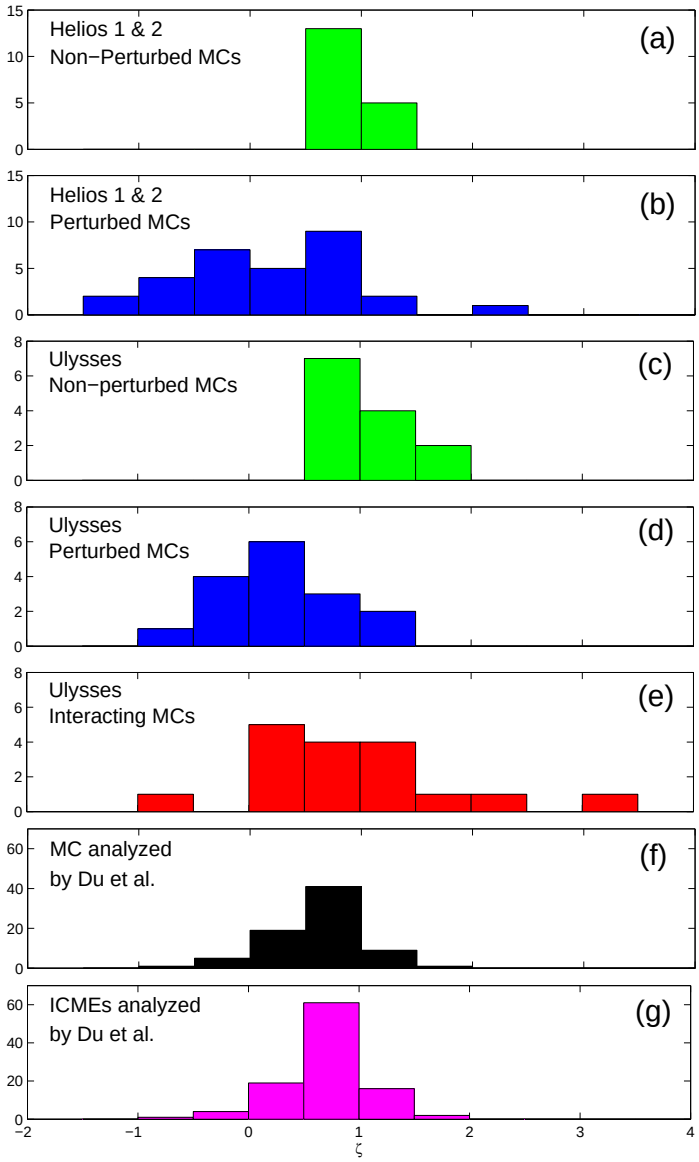

Fig. 7. Histograms comparing ζ of MCs and non-MC ICMEs. **(a,b)** MCs from Helios spacecraft (Gulisano et al. 2010). **(c-e)** MCs from Ulysses spacecraft (present work). **(f,g)** MCs and non-MC ICMEs from Ulysses with approximative ζ values computed from the results of Du et al. (2010).

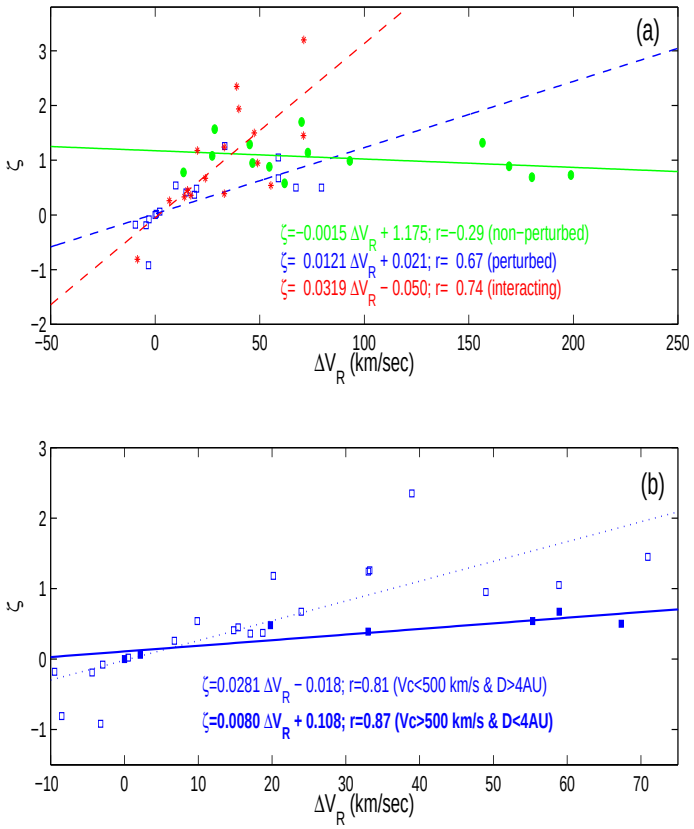

Fig. 8. Perturbed and non-perturbed MCs have a remarkably different behavior of ζ when they are plotted as a function of ΔV_R. The drawing convention is the same than in Fig. 4 for panel **(a)** while the perturbed MCs are grouped by velocity and distance in panel **(b)** as indicated by the legend.

$S_{1\,\mathrm{AU}}$ and $< B >_{1\,\mathrm{AU}}$ have similar ranges for Helios and Ulysses MCs.

As for Helios MCs, ζ does not depend on the expansion velocity ΔV_R [defined by Eq. (4)] for non-perturbed MCs observed by Ulysses, while ζ is strongly correlated with ΔV_R for perturbed MCs (compare Fig. 8a with Fig. 5 in Gulisano et al. 2010). This result extends previous Helios results to large distances. Indeed non-perturbed MCs have an intrinsic expansion rate ζ (which is given by the decrease of the total SW pressure with solar distance). This is not the case of perturbed MCs which are in a transient stage, so ΔV_R cannot be computed by $\mathrm{d}S/\mathrm{d}t$ as done in Eq. (7). Rather, following the derivation of Gulisano et al. (2010):

$$\zeta_{\mathrm{perturbed}} = \frac{\Delta V_R}{S}\frac{D}{V_c} \approx \frac{\Delta V_R D_0^m D^{1-m}}{S_0 V_c}\,, \qquad (9)$$

where the MC size S_0 is taken at distance D_0. Then, for perturbed MCs one expects a linear dependance of ζ with ΔV_R, what is indeed present (Fig. 8a). Interacting MCs are strongly perturbed, and indeed they have a stronger dependance of ζ with ΔV_R.

Moreover, from Eq. (9), an expected dependance on D and V_c is expected. Within the observed ranges, both parameters have a comparable effect on the slope. Since we have a too low number of MCs to perform a dependance test on both D and V_c, we only considered the two groups where D and V_c cumulate their effect on the slopes. So these two groups have larger slope differences, and luckily, they are also the most numerous groups. The first group is defined by $V_c < 500$ km/s and $D > 4$ AU; it has $< V_c > \approx 410$ km/s and $< D > \approx 5.1$ AU. The second group is defined by $V_c > 500$ km/s and $D < 4$ AU; it has $< V_c > \approx 640$ km/s and $< D > \approx 2.6$ AU. We use a typical $S_0 = 0.2$ AU value at $D_0 = 1$ AU, and $m = 0.54$ as found for perturbed MCs (Table 1). The first group has an expected slope of 0.026 which is comparable to the one derived from the data (0.028, Fig. 8b). The second group has a smaller expected slope of 0.012 and the observations give a slope even lower by a factor 1.5. One can also compare the ratio of predicted and observed slopes to eliminate the influence of S_0: the observed ratio of slopes is a factor 1.6 higher than the predicted one, and it decreases to 1.4 if we use $m = 0.28$, the mean ζ value found for perturbed MCs (Table 2). Taken into account the uncertainties on the MC parameters, these results indeed show that Eq. (9) provides a quantitative dependance of ζ with D and V_c for perturbed MCs.

4.4. Global radial expansion

The determination of ζ provides the expansion rate of the MC at the time of the observations while its size S depends on the past history of ζ. If S would be observed at another solar distance, this would provide a global information on the expansion between the two distances (as well as another local information of ζ). However, the observation of the same MC by two spacecraft is a rare event since it requires a close alignment of the spacecraft positions with the propagation direction of the MC (one case is analyzed by Nakwacki et al. 2011). Still, the statistical evolution of S with D provides a constraint on the mean evolution of MCs. The flux rope size of non-perturbed MCs have a mean dependence close to (Fig. 4a)

$$S \propto D^{0.79\pm0.46}. \quad (10)$$

If a MC evolves with ζ constant, it implies $S \propto D^{\zeta}$ (Sect. 4.1). The non-perturbed MCs are expected to have the most stable ζ value. Their mean ζ value, 1.05 ± 0.34 (Table 2), indicates that they are in a faster expanding stage than the global results of Eq. (10). The possible difference is that the flux rope size decreases with distance due to reconnection with the encountered SW magnetic field. The observed trace of this reconnection is the presence of a back region in a large majority of MCs (e.g. a back region is present in the three MCs shown in Figs. 1,2). Indeed, if the flux rope size would decrease by a factor ≈ 1.5 between 1.4 and 5.4 following a power-law of D, it would decrease S by $D^{0.3}$, so sufficiently to explain the above difference between the mean evolution of S [Eq. (10)] and $< \zeta >$ for non-perturbed MCs.

An alternative possibility is that, at least, part of the non-perturbed MCs were in fact previously perturbed so that their ζ value was lower. This would imply a lower global expansion of the MC, so a lower dependence of S on D. Indeed, $< \zeta >= 0.77 \pm 0.75$ for non-perturbed, perturbed, and interacting MCs taken together, which is much closer to the exponent in Eq. (10) than $< \zeta >$ for the unperturbed MCs alone. In this view, the unperturbed, interacting, and perturbed classification is a local one, only valid around the time of the observation and, a MC is changing of group (non-perturbed/**perturbed**/interacting) as it travels away from the Sun. Finally, both possibilities mentioned above could well be present.

4.5. MC and ICME expansion

In this section we analyze a broader set of MCs and ICMEs from the results published by Du et al. (2010). They defined ICMEs following Wang et al. (2005b) as the time intervals where the proton temperature, T_p, was less than half the expected temperature in the SW with the same speed. They found that about 43% of the identified ICMEs are MCs. Their Ulysses data set covers the time interval from January 1991 to February 2008. The main mean parameters of this data set are given in Table 2. Both groups have similar characteristics than the MCs studied in this paper, with the exception of a significantly lower magnetic field strength in non-MC ICMEs.

Du et al. (2010) performed a linear fit of the radial velocity through the full ICME (defined by T_p, while we restrict to inside the flux rope for our study). They defined ΔV as the speed difference between the leading and trailing edges of the ICME. The distribution of ΔV is closely similar between MCs and non-MC ICMEs (Du et al. 2010, Fig. 4). The main differences are only that few MCs have a large ΔV and that more non-MC ICMEs have very low ΔV.

In their table of ICMEs, Du et al. (2010) provided all the quantities to compute ζ [Eq. (5)]. We find Gaussian-shaped histograms of ζ for both MCs and non-MC ICMEs (Fig. 7f,g). They are very similar, in particular their mean and dispersion are comparable ($\zeta = 0.59 \pm 0.51$ for MCs and $\zeta = 0.68 \pm 0.48$ for non-MC ICMEs). This is compatible with a common idea that non-MC ICMEs have the same properties as MCs, but they are simply observed *in situ* near their periphery in such a way that the internal flux rope is missed.

These results are also comparable to our results when we group all MCs together and even more when we consider non-perturbed and perturbed MCs (Fig. 7, Table 2). However, our detailed analysis permits to separate MCs which are in different conditions. The MCs in interaction have the broader range of ζ (Fig. 7e) since they are strongly affected by the interaction, and they are observed at different times of the interaction process. The non-perturbed MCs have logically the less dispersion of ζ (Fig. 7c). So behind the dispersion of ζ found from Du et al. (2010) results, different environments or/and evolution stages are present.

5. MCs in interaction

5.1. Evolution of MCs in a complex solar wind

Some MCs are traveling in a structured SW formed by plasma coming from different parts of the solar corona. Such plasmas have different properties, e.g. plasma speed and magnetic field, so they are interacting. For example, a rarefaction region is formed when a fast SW is preceding a slow SW while a compression region is formed when a fast SW overtakes a slow SW. Moreover, especially around the maximum of the solar cycle, several ICMEs could be ejected from the Sun at similar times, then they could interact later on. When a MC is traveling in a structured SW, the encountered structures affect its evolution.

The group of perturbed MCs, analyzed above, are interpreted as examples of such MCs affected during their travel from the Sun by the encountered SW structures. However, since it was mostly a past interaction, there is no direct evidence of the interaction in the *in situ* data. The past interaction for such MCs is only suspected by the presence of an overtaking flow and by a typically lower ζ value. For some other MCs, the interaction is still taking place during the observations. In such a case, the MC evolution depends on the type of interaction (e.g. on the external structure involved, the relative velocity, the magnitude of its plasma parameters and field strength) as well as the time elapsed since the beginning of the interaction. It implies that the study of MCs in interaction needs to be done typically as a case by case study. We include the MCs with a strong interaction at the time of their in situ observation, in a third group (called simply interacting). In the next two subsections, we analyze two sub-groups (called I_B and I_{MC}) of such interacting MCs.

5.2. MCs with stronger B-field nearby

In the first sub-group, I_B, MCs have a strong magnetic field in their surroundings, typically stronger by a factor above 1.5 than the mean field strength inside the MC. However, this sub-group contains only cases where the nearby magnetic structure has not the characteristics of a MC.

MCs 21 and 46 both have a strong magnetic field within a large front sheath (larger than the MC size). Both have a low ζ value (0.26 and 0.39 respectively). MCs 4 and 27 both have a strong magnetic field behind them within an extended region

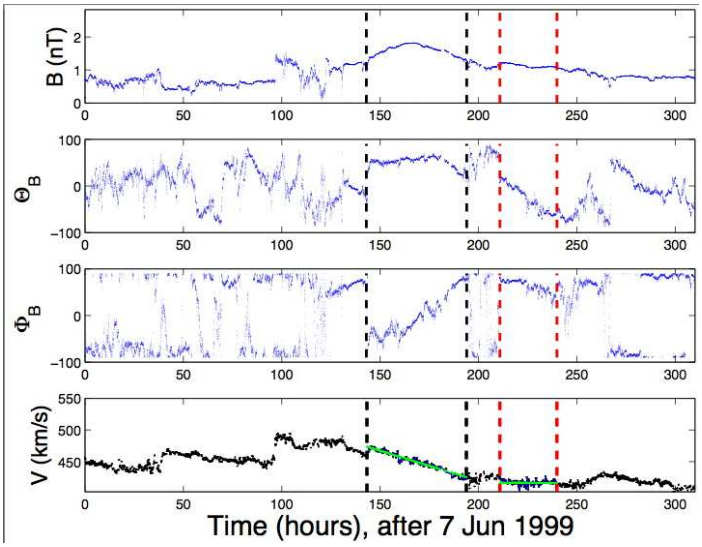

Fig. 9. Example of two MCs in interaction. MC 44 is a large MC with a strong magnetic field; it is followed by the smaller MC 26 (the vertical dashed lines define the MC boundaries). The magnetic field rotation is mostly in the longitude of the field (Φ_B) for MC 44 and mostly in the latitude of the field (θ_B) for MC 26 showing that the MC axis are almost orthogonal. Still there is only a weak change of the magnetic field between the out-bound branch of MC 44 and the in-bound branch of MC 26. The MCs are separated by a sheath-like region with a magnetic field of different orientation. The bottom panel shows that MC 26 is not expanding. A linear least square fit of the velocity is shown with a green line in the time interval where an almost linear trend is present in each MC.

(larger than the MC size). Both MCs have a field strength increasing from the front to the rear, and this is especially marked for MC 27 since its B-profile is unusually increasing almost linearly from the front to the rear by a factor $\approx$ 2. MC 4 has a relatively small ζ value (0.54) while MC 27 is in compression ($\zeta = -0.81$). MCs 10 and 33 have also a strong magnetic field behind them, while at the difference of both previous MCs, their internal field strength has rather several unusual structures showing that they are strongly perturbed. They are both expanding less than average as $\zeta = 0.36$ and 0.33, respectively.

We conclude that the above 6 MCs are compressed by the surrounding strong magnetic pressure so that they are expending less than average (even one MC is in a strong compression stage). However, there is one exception, MC 1 which has also a strong magnetic field behind (in a region more extended than the MC size) but it is in over-expansion as $\zeta = 1.45$. This MC is likely to be in a late interaction stage where the internal pressure, build up previously in the under expansion stage, becomes too large so that it could drive an over expansion (see Sect. 4.3).

5.3. Interacting MCs

When, after the solar eruption of a magnetic cloud, another one is ejected with faster velocity and in similar direction than the first one, an interaction between the two MCs is expected near their encounter time. Depending of the relative orientation of the magnetic field of the two interacting MCs, magnetic reconnection can develop during the interaction. Previous studies of these processes have been done using observations of individual studied cases for both, favorable conditions to the magnetic reconnection (e.g., Wang et al. 2005a), as well for non-reconnection conditions (e.g., Dasso et al. 2009). The dynamical evolution during the interaction of two magnetic clouds have been also studied numerically from MHD simulations (e.g., Lugaz et al. 2005; Xiong et al. 2007). These studies have typically found that a linear velocity profile is reached in the late evolution phase when the two MCs are traveling together.

We analyze such interacting MCs, with at least another MC in their vicinity, in the second subset of interacting MCs (I_{MC}). An example is shown in Fig. 9. The large MC 44 has a typical expanding rate ($\zeta = 0.95$) while the smaller MC 26 located behind has no significant expansion ($\zeta \approx 0.$). A second couple of MCs have similar magnetic field strength ($< B > \approx 1$ nT), and the front MC 18 is in slight over expansion ($\zeta = 1.24$) while, behind, MC 19 is in under expansion ($\zeta = 0.45$). A third couple of MCs is formed by MCs 15 and 42. MC 15 was also detected by ACE spacecraft at 1 AU. Its expansion rate was classical ($\zeta = 0.74$, Nakwacki et al. 2011). However, when the same MC is measured at 5.4 AU, it is strongly overtaken. In particular, its out-bound branch is compressed ($< B > \approx 1.2$ nT compared to $< B > \approx 0.5$ nT in its in-bound branch) and in under expansion ($\zeta \approx 0.57$ compared to $\zeta = 0.67$ in its in-bound branch). This MC 15 is overtaken by MC 42 which has a much stronger field ($< B > \approx 3$ nT) and which is in strong over expansion ($\zeta = 2.35$).

Finally, the data set contains three MCs traveling close by. The three MCs (7,41,8) have similar field strength, and this triad was identified as one ICME by Funsten et al. (1999) with an interval of counter streaming electrons covering the full duration of the triad. All MCs are in over expansion ($\zeta = 3.2$, 1.94, 1.5, respectively), while the triad taken as a whole has an expansion rate closer to the mean value of all the MCs ($\zeta \approx 0.8$). Since this last ζ value is very different than the ζ values found inside each MCs, this triad of MCs is far from a relaxation state with a linear profile for the full time period (in contrast of the results of numerical simulations). In the same line, the three couple of MCs analyzed above also show significant difference of ζ values as illustrated for one couple in Fig. 9.

The above three pairs and one triad of interacting MCs show a variety of cases. This contrast with the simple evolution found in MHD simulations between similar flux ropes, as follows. As with an overtaking fast flow, the MC in front is first compressed, so its expansion rate decreases (Lugaz et al. 2005; Xiong et al. 2007). The couple of MCs 18,19, with similar field strength and size, is the closest from these simulations. However, the following MC is in under expansion while it is the leading one in MHD simulations.

In the case where magnetic reconnection is inhibited between the flux ropes (by nearly parallel magnetic fields), later on in the MHD simulations the couple of MCs travels together forming only one expanding structure, i.e. with a nearly linear velocity profile across both MCs (see Fig. 4 of Xiong et al. 2007). Such case was not found in present data case.

Other MHD simulations have shown a more complex velocity pattern, for example in the case of the interaction of three flux ropes (see Fig. 6 of Lugaz et al. 2007). Still we are missing a complete view of the interaction of MCs of various sizes, orientations and magnetic helicities to interpret the above observed interacting MCs. We are also missing the history of the interaction, and this is crucial for understanding the local measurements since the above MHD simulations have shown that the interaction is a time-depend process (even in the simplest interaction cases). Part of the history can be provided by other data such as heliospheric imagers and interplanetary radio data for a more recent time period of analysis (with STEREO spacecraft).

6. Summary and Conclusions

The main goal of present paper is to investigate how the MCs properties, in particular the expansion rate, evolve in the outer heliosphere from what is known in the inner heliosphere and at 1 AU from previous studies. During the travel from the Sun to the location of the *in situ* observations, the MC field could be partially reconnected with the overtaking magnetic field, as evidenced by the presence of a back region in a large fraction of MCs. We define the MC boundaries to retain only the remaining flux rope part in order to analyze only the region which is not mixed with the SW.

Each observed MC has its own properties, with different temporal profiles of its magnetic field and its plasma parameters. We still find similarities between MCs which allow us to define three MC groups. The MCs within the first group have a radial velocity profile almost linear with time, indicating a self-similar expansion as theoretically expected, so this group is called non-perturbed (see examples in Fig. 1). In the second group, the temporal velocity profile could have significant deviation from linearity, so they are perturbed (see examples in Fig. 2). Finally, we consider separately the MCs which have a large magnetic field structure nearby and they are defined as the group in interaction (one example is shown in Fig. 9).

The perturbed MCs have an average size lower than for the non-perturbed MCs (Fig. 4a), while it is the opposite for the magnetic field strength, the proton density and temperature (Fig. 4b,c,5a). All these results are coherent with perturbed MCs less expanding with solar distance than non-perturbed MCs, a property which is indeed found independently from the analyzed of the *in situ* proton velocity (Fig. 6). For the proton β, we found no significant difference between these two MC groups (Fig. 5b).

The expansion in the radial direction (away from the Sun) is characterized with the non-dimensioned parameter ζ, defined by Eq. (5) from the *in situ* velocity profile. When the observed velocity profile is linear with time, the MC size has a power-law expansion such as $S \sim D^{\zeta}$ [Eq. (6) and following text]. For non-perturbed MCs, ζ has a narrow distribution ($\zeta = 1.05 \pm 0.34$). This is slightly above the value found in the inner heliosphere (0.91 ± 0.23) and at 1 AU (0.80 ± 0.18). This is also larger than the global expansion exponent found from the analysis of the MC size versus helio-distance (0.79 ± 0.46). This lower exponent for the size could be due to the progressive pealing of the flux rope by reconnection or/and to a temporal evolution (Sect. 4.4).

The expansion rate of perturbed MCs, $\zeta = 0.28 \pm 0.52$, is in average significantly lower than for non-perturbed MCs, in quantitative agreement with previous results in the inner heliosphere. ζ is also more variable within the group of perturbed MCs, as in the inner heliosphere, with even one MC in over expansion. These results are in agreement with a temporal evolution of the expansion rate during the interaction with an overtaking flow as found in MHD simulations.

The MCs in interaction with a stronger magnetic field region have the largest variety of expansion rates $\zeta = 1.00 \pm 0.93$. Some of these MCs are in a large expansion stage (up to a factor 3 larger than for non-perturbed MCs), while one MC is even in compression. Such variety of expansion rate is partially present in MHD simulations of interacting flux ropes or a flux rope overtaken by a fast stream: there is first a compression at the beginning of the interaction, followed by an increasing expansion rate which could reach an over expansion much latter on (with a magnitude which remains to be quantified). Still the properties of MCs in interaction are difficult to interpret both because the past history is unknown and because they show a larger variety than in MHD simulations.

Appendix A: List of studied MCs

The studied MCs are listed in Table A.1. We added the MCs 41 to 46, which were not present in the list of Rodriguez et al. (2004).

Acknowledgements. The authors acknowledge financial support from ECOS-Sud through their cooperative science program (N^o A08U01). This work was partially supported by the Argentinean grants: UBACyT 20020090100264, PIP 11220090100825/10 (CONICET), and PICT-2007-856 (ANPCyT). S.D. is member of the Carrera del Investigador Científico, CONICET. S.D. acknowledges support from the Abdus Salam International Centre for Theoretical Physics (ICTP), as provided in the frame of his regular associateship. L.R. acknowledges support from the Belgian Federal Science Policy Office through the ESA-PRODEX program, and the European Union Seventh Framework Programme (FP7/2007-2013) under grant agreement number 263252 [COMESEP].

References

Balogh, A., Beek, T. J., Forsyth, R. J., et al. 1992, A&AS, 92, 221
Bame, S. J., McComas, D. J., Barraclough, B. L., et al. 1992, A&AS, 92, 237
Bothmer, V. & Schwenn, R. 1998, Annales Geophysicae, 16, 1
Burlaga, L. F. 1995, Interplanetary magnetohydrodynamics (Oxford University Press, New York)
Cane, H. V. & Richardson, I. G. 2003, J. Geophys. Res., 108, 1156
Cane, H. V., Richardson, I. G., & Cyr, O. C. S. 2000, Geophys. Res. Lett., 27, 3591
Chen, J. 1996, J. Geophys. Res., 101, 27499
Dasso, S., Mandrini, C. H., Démoulin, P., & Luoni, M. L. 2006, A&A, 455, 349
Dasso, S., Mandrini, C. H., Schmieder, B., et al. 2009, J. Geophys. Res., 114, A02109
Dasso, S., Nakwacki, M. S., Démoulin, P., & Mandrini, C. H. 2007, Sol. Phys., 244, 115
Démoulin, P. & Dasso, S. 2009a, A&A, 498, 551
Démoulin, P. & Dasso, S. 2009b, A&A, 507, 969
Démoulin, P., Nakwacki, M. S., Dasso, S., & Mandrini, C. H. 2008, Sol. Phys., 250, 347
Du, D., Zuo, P. B., & Zhang, X. X. 2010, Sol. Phys., 262, 171
Farrugia, C. J., Burlaga, L. F., Osherovich, V. A., et al. 1993, J. Geophys. Res., 98, 7621
Fränz, M. & Harper, D. 2002, Planet. Space Sci., 50, 217
Funsten, H. O., Gosling, J. T., Riley, P., et al. 1999, J. Geophys. Res., 104, 6679
Gazis, P. R., Balogh, A., Dalla, S., et al. 2006, Space Sci. Rev., 123, 417
Gosling, J. T., McComas, D. J., Phillips, J. L., & Bame, S. J. 1991, J. Geophys. Res., 96, 7831
Gulisano, A. M., Dasso, S., Mandrini, C. H., & Démoulin, P. 2007, Adv. Spa. Res., 40, 1881
Gulisano, A. M., Démoulin, P., Dasso, S., Ruiz, M. E., & Marsch, E. 2010, A&A, 509, A39
Klein, L. W. & Burlaga, L. F. 1982, J. Geophys. Res., 87, 613
Kumar, A. & Rust, D. M. 1996, J. Geophys. Res., 101, 15677
Leitner, M., Farrugia, C. J., Möstl, C., et al. 2007, J. Geophys. Res., 112, A06113
Lepping, R. P., Berdichevsky, D. B., Szabo, A., Arqueros, C., & Lazarus, A. J. 2003, Sol. Phys., 212, 425
Liu, Y., Richardson, J. D., & Belcher, J. W. 2005, Planet. Space Sci., 53, 3
Lopez, R. E. & Freeman, J. W. 1986, J. Geophys. Res., 91, 1701
Low, B. C. 1997, in Coronal Mass Ejection, Geophys. Monograph 99, 39–48
Lugaz, N., Manchester, IV, W. B., & Gombosi, T. I. 2005, ApJ, 634, 651
Lugaz, N., Manchester, IV, W. B., Roussev, I. I., Toth, G., & Gombosi, T. I. 2007, ApJ, 659, 788
Nakwacki, M., Dasso, S., Démoulin, P., Mandrini, C. H., & Gulisano, A. M. 2011, A&A, 535, A52
Richardson, I. G. & Cane, H. V. 1995, J. Geophys. Res., 100, 23397
Rodriguez, L., Woch, J., Krupp, N., et al. 2004, J. Geophys. Res., 109, A01108
Rust, D. M. 1994, Geophys. Res. Lett., 21, 241
Shimazu, H. & Vandas, M. 2002, Earth, Planets, and Space, 54, 783
St. Cyr, O. C., Plunkett, S. P., Michels, D. J., et al. 2000, J. Geophys. Res., 105, 18169
Steed, K., Owen, C. J., Démoulin, P., & Dasso, S. 2011, J. Geophys. Res., 116, A01106
Tsurutani, B. T., Smith, E. J., Gonzalez, W. D., Tang, F., & Akasofu, S. I. 1988, J. Geophys. Res., 93, 8519

Table A.1. List of MCs and their main properties.

MC[a]	t_c [b] d-m-y h:m (UT)	Group [c]	θ [d] °	D [d] AU	V_c [e] km/s	S [e] AU	$< B >$ [f] nT	$< N_p >$ [f] cm^{-3}	$< \beta_p >$ [f]	γ [g] °	ζ [h]
1	17-Jul-1992 19:46	interacting	-14	5.3	447	0.58	0.83	0.10	0.14	60	1.45
2	15-Nov-1992 23:18	perturbed	-20	5.2	595	1.39	0.91	0.04	0.12	82	0.50
3	11-Jun-1993 18:29	non-perturbed	-32	4.6	728	1.65	0.98	0.05	0.14	79	0.69
4	10-Feb-1994 16:46	interacting	-52	3.6	723	0.51	1.55	0.17	0.24	74	0.54
5	3-Feb-1995 21:05	perturbed	-22	1.4	754	0.25	4.33	1.26	0.21	55	0.50
6	15-Oct-1996 01:55	non-perturbed	24	4.6	673	1.30	0.64	0.04	0.11	67	0.89
7	10-Dec-1996 20:04	interacting	21	4.6	601	0.17	0.91	0.10	0.34	48	3.20
8	12-Dec-1996 22:45	interacting	20	4.7	512	0.29	0.94	0.14	0.31	65	1.50
9	09-Jan-1997 09:35	perturbed	19	4.7	471	0.36	2.05	0.42	0.10	40	0.41
10	27-May-1997 01:52	interacting	10	5.1	439	0.55	0.98	0.19	0.21	80	0.36
11	17-Aug-1997 09:59	perturbed	6	5.2	361	0.73	1.47	0.25	0.08	79	0.37
12	30-Aug-1997 19:26	perturbed	5	5.2	392	0.35	1.58	0.40	0.18	71	1.26
13	14-Nov-1997 19:18	non-perturbed	2	5.3	387	0.48	1.04	0.29	0.25	80	1.29
14	25-Jan-1998 20:24	perturbed	-2	5.4	379	0.05	1.72	0.24	0.08	53	-0.92
15	26-Mar-1998 22:53	interacting	-29	5.4	351	1.10	0.48	0.12	0.37	89	0.67
16	09-Apr-1998 20:34	perturbed	-6	5.4	411	0.24	0.58	0.36	0.71	68	0.54
17	15-Aug-1998 02:24	perturbed	-12	5.4	444	0.64	2.34	0.58	0.44	90	-0.18
18	27-Aug-1998 00:02	interacting	-13	5.4	389	0.37	0.91	0.16	0.15	73	1.24
19	30-Aug-1998 07:15	interacting	-13	5.4	377	0.49	1.10	0.22	0.16	71	0.45
20	8-Sep-1998 23:16	non-perturbed	-13	5.3	372	0.36	0.51	0.12	0.27	41	1.08
21	19-Sep-1998 02:19	interacting	-14	5.3	363	0.38	0.90	0.27	0.28	64	0.26
22	8-Oct-1998 16:35	non-perturbed	-15	5.3	401	0.82	0.95	0.04	0.03	85	0.88
23	9-Nov-1998 00:53	non-perturbed	-16	5.3	426	1.17	1.03	0.18	0.15	89	0.99
24	12-Nov-1998 16:16	interacting	-16	5.3	412	0.22	1.24	0.23	0.16	60	1.18
25	5-Mar-1999 01:18	perturbed	-22	5.1	454	0.63	2.72	0.27	0.14	86	1.05
26	16-Jun-1999 08:22	perturbed	-28	4.8	417	0.29	1.13	0.65	0.04	88	0.02
27	17-Aug-1999 06:46	interacting	-32	4.7	411	0.12	1.21	0.48	0.24	74	-0.81
28	31-Mar-2000 21:32	non-perturbed	-50	3.7	401	0.16	6.12	2.01	0.07	73	0.78
29	15-Jul-2000 14:52	non-perturbed	-62	3.2	500	0.41	0.29	0.06	0.73	21	1.14
30	11-Aug-2000 06:22	non-perturbed	-66	3.0	459	0.32	1.35	0.43	0.11	85	0.95
31	6-Dec-2000 23:15	non-perturbed	-80	2.2	394	0.23	2.84	0.80	0.08	31	1.70
32	12-Apr-2001 01:28	non-perturbed	-26	1.4	593	0.28	5.95	1.47	0.07	87	1.32
33	7-Jul-2001 13:35	interacting	40	1.4	296	0.20	4.18	8.51	0.67	81	0.33
34	24-Jul-2001 04:36	non-perturbed	51	1.5	381	0.42	5.17	2.39	0.16	30	0.58
35	24-Aug-2001 19:09	perturbed	68	1.7	539	0.13	8.78	2.70	0.06	88	0.48
36	14-Nov-2001 22:53	perturbed	75	2.3	632	0.32	2.77	0.18	0.03	79	0.67
37	12-Feb-2002 13:32	perturbed	58	2.9	519	0.20	4.73	1.76	0.11	58	0.06
38	5-May-2002 15:02	non-perturbed	46	3.4	385	0.16	1.87	0.82	0.09	70	1.57
39	16-Jun-2002 21:19	non-perturbed	41	3.6	658	1.49	2.85	0.17	0.02	70	0.73
40	18-Jul-2002 06:51	perturbed	38	3.8	530	0.08	3.54	0.51	0.04	79	0.00
41	11-Dec-1996 15:18	interacting	20	4.6	558	0.17	0.85	0.07	0.12	55	1.94
42	29-Mar-1998 07:06	interacting	-5	5.4	358	0.25	2.93	0.94	0.14	59	2.35
43	20-Apr-1998 12:38	perturbed	-6	5.4	416	0.30	1.64	0.28	0.13	65	-0.19
44	14-jun-1999 10:42	interacting	-28	4.8	450	0.55	1.60	0.21	0.09	58	0.95
45	17-Jan-2000 12:09	perturbed	-44	4.1	398	0.38	2.01	1.05	0.51	68	-0.08
46	27-Nov-2001 19:47	interacting	73	2.3	779	0.25	2.34	0.23	0.16	37	0.39

[a] Number identifying MCs.
[b] t_c is the time of closest approach from the MC axis.
[c] The MCs are separated in three groups: non-perturbed, perturbed, and in interaction (noted interacting).
[d] θ and D are the latitude and solar distance.
[e] V_{ξ} is the velocity at the closest distance from the MC axis and S is the MC size. Both are computed in the radial direction away from the Sun ($\hat{\mathbf{R}}$).
[f] $< B >$, $< N_p >$ and $< \beta_p >$ are the average over the flux rope of the field strength, the proton density and the proton β, respectively.
[g] γ is the acute angle between the MC axis and the radial direction ($\hat{\mathbf{R}}$).
[h] ζ is the unidimensional expansion rate [Eq. (5)]. $\zeta < 0$ means a MC observed in compression stage.

Wang, A. H., Wu, S. T., & Gopalswamy, N. 2005a, *Geophysical Monographs 156, AGU*, 185
Wang, C., Du, D., & Richardson, J. D. 2005b, J. Geophys. Res., 110, A10107
Webb, D. F., Cliver, E. W., Crooker, N. U., Cry, O. C. S., & Thompson, B. J. 2000, J. Geophys. Res., 105, 7491
Xiong, M., Zheng, H., Wang, Y., & Wang, S. 2006a, J. Geophys. Res., 111, A08105
Xiong, M., Zheng, H., Wang, Y., & Wang, S. 2006b, J. Geophys. Res., 111, A11102
Xiong, M., Zheng, H., Wu, S. T., Wang, Y., & Wang, S. 2007, J. Geophys. Res., 112, A11103